Electrochemistry Communications 140 (2022) 107325

Contents lists available at ScienceDirect

Electrochemistry Communications

journal homepage: www.elsevier.com/locate/elecom

A biomass-based cathode for long-life lithium-sulfur batteries

Jian Yang [a], Guanyi Wang [a], Ana Paula Teixeira [b], Glaura Goulart Silva [b], Zachary Hansen [a], Maruj Jamal M Jamal [a], Kevin Mathew [a], Jie Xiong [a], Tiffany Zhou [a], Michal Mackowiak [c], Paul Dan Fleming [a], Qingliu Wu [a,*]

[a] Department of Chemical and Paper Engineering, Western Michigan University, 4601 Campus Drive, Kalamazoo, MI 49008-5462, USA
[b] Centro de Tecnologia em Nanomateriais e Grafeno CTNano, Federal University of Minas Gerais, Belo Horizonte-MG, Brazil
[c] Xponential Battery Materials, Amsterdam, Netherlands

ARTICLE INFO

Keywords:
Biomass
Porous carbon
Lithium-sulfur battery

ABSTRACT

With the advantages of high conductivity and low cost, porous carbons have been considered as the most attractive host materials of sulfur cathodes in lithium-sulfur batteries (LSBs). However, LSBs always suffer short cycle life due to the "shuttle effect" of lithium polysulfide species (polysulfides), which are intermediate products during the charge/discharge processes. The weak interaction between carbon and polysulfides results in the dissolution of polysulfides from the cathodes, loss of active material of sulfur and eventually fast capacity fading. To overcome these drawbacks, we employed a biomass-derived carbon as the host material in sulfur cathodes. Results from X-ray diffraction (XRD), scanning electron microscopy (SEM) and nitrogen sorption reveals that this biomass-derived product is amorphous carbon and is composed of both large (>10 nm) and small (<5 nm) pores at an appropriate ratio. Using as hosts of cathodes in LSBs, the biomass-derived carbons deliver a high reversible capacity of >800 mAh/g and retain >80% of initial capacity after 200 cycles. Especially, the activated carbons exhibited an unprecedently high durability with 80% capacity retention after 400 cycles. The promising LSB performance can be ascribed to the unique porous architecture of biomass-derived carbons. The small pores in biomass-derived carbons provide more sites to anchor sulfur and polysulfides, while large pores provide channels for fast transport of ions. This is corroborated by the results from the electrochemical impedance spectroscopy (EIS), the thermogravimetric analysis (TGA) and absorption measurements.

1. Introduction

With the advantages of high electronic conductivity and low cost, the carbonaceous materials have been considered as the most attractive hosts of sulfur cathodes in lithium-sulfur batteries (LSBs) [1–4]. However, the derived LSBs always suffer the fast capacity decay due to the "shuttle effect" of soluble lithium polysulfide species (polysulfides), which are intermediate products during the charge/discharge processes, arising from the weak interaction between carbon and polysulfides. This promotes the efforts on developing advanced carbon-based hosts, such as nanostructured carbons with confining effect and carbon composites with chemical affinity to polysulfides. Successful examples including carbon nanotubes (CNTs) [5–9], micro/mesoporous carbon spheres [10–14], porous carbon with functional groups [15,16]and metal oxides/sulfides/nitrides decorated carbons [7,9,17–21] greatly elongate the cycle life of derived LSBs. However, the complexity of fabricating processes [6,12,22] and the high cost of special precursors [16,19,23] limit the commercialization of LSBs with advanced carbon-based hosts. Therefore, there is a critical need to develop a new carbonaceous host with low cost and strong constrains to polysulfides to booster the LSB performance and thus accelerate its wide adoption to the electronic device market.

The biomass-derived carbon possesses the advantages of large specific surface area (SSA), high porosity and low cost, and has been considered as one of the most promising host materials [24,25] since it was first employed as the host of sulfur cathode in LSBs in 2011 [26]. The large SSA can enhance the sulfur content, improve the dispersion of elemental sulfur in the conductive carbon matrix, and thus increase the utilization of sulfur [27]. However, the SSA of carbon materials has little effect on alleviating the polysulfide dissolution. The small pores, especially micropores (pore width of < 2 nm), can provide spatial constrains, mitigate the polysulfide dissolution from the sulfur cathodes and

* Corresponding author.
E-mail address: qingliu.wu@wmich.edu (Q. Wu).

https://doi.org/10.1016/j.elecom.2022.107325
Received 20 May 2022; Received in revised form 11 July 2022; Accepted 13 July 2022
Available online 20 July 2022

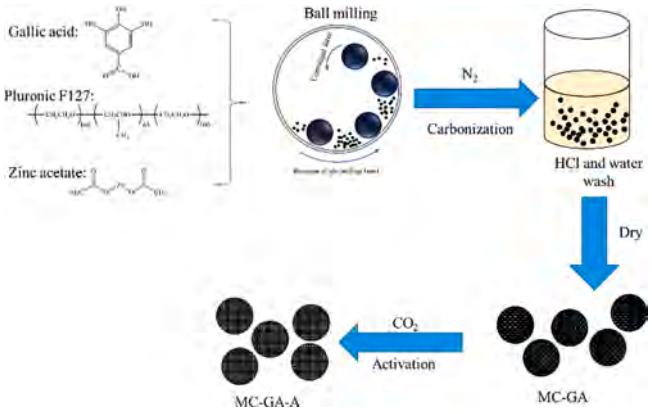

Fig. 1. Schematic illustration of the approach to fabricate biomass-derived porous carbon.

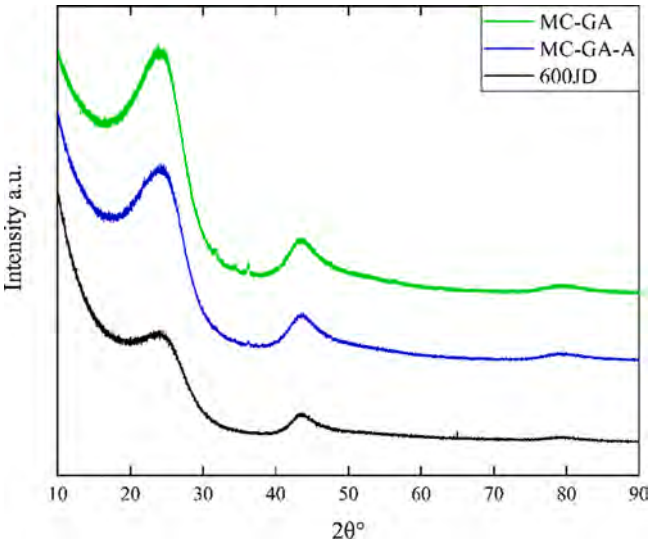

Fig. 2. XRD patterns of porous carbons.

eventually improve the durability of LSBs [28]. For instance, the microporous graphic carbon (MGC) synthesized from peanut shell has the predominant pore width <0.4 nm and the strong confinement of polysulfides in the micropores enables the derived LSBs the high capacity of 826 mAh/g at 1C after 1000 cycles [29]. However, the low pore volume limits the mass ratio of sulfur loaded into the cathodes and the utilization of sulfur at high rates. Therefore, it is necessary to develop a biomass-derived carbon host having balanced trapping ability and utilization of active material for energy-dense LSBs with long cycle life.

It has been well recognized that the porous architecture of biomass-derived carbons plays a crucial role in determining the LSB performance. The small pores (micropores) have strong absorption to polysulfides [30], while large pores (mesopores with pore width of 2–50 nm) allow the high sulfur load [31] and provide channels for the ion diffusion [32]. In light of this, carbonaceous hosts possessing both micropores and mesopores and an appropriate pore size distribution (or volume ratio between micropore and mesopore) can make derived sulfur cathodes exhibit high sulfur utilization and strong trapping capability to polysulfides. This has been confirmed by the excellent performance of LSBs containing biomass-derived carbon hosts with hierarchically porous architectures [30–33]. These prior achievements inspired us to develop a new carbon with dual porosity from gallic acid (GA) and use it as the host material for high performance LSBs. As a member in the biomass family, GA is one of the main natural phenolic components widely presented in plants [34] and has the advantages of low cost, low toxicity and natural abundance [35]. As the supercapacitor electrodes, GA-derived porous carbon exhibited the highest electrical conductivity among different types of plant-derived polyphenols [36]. Therefore, it is rational to anticipate that the sulfur cathodes with GA-derived carbon hosts will inherit these advantages and render LSBs promising performance.

Here, we synthesized a new porous carbon with dual porosity via a solvent-free approach with GA as the carbon source. The properties of obtained porous carbon were characterized. Used as the host of sulfur cathode, the promises of GA-derived carbon host in improving the LSB performance were demonstrated and the effect of porous structure on the LSB performance was discussed.

2. Material and methods

2.1. Material preparation

The porous carbons were prepared through a solvent-free synthesis approach, as shown in Fig. 1. GA was used as a carbon source, the Pluronic surfactant F127 was used as a soft template, and zinc acetate was used as a crosslinking agent. The precursor GA, the Pluronic surfactant F127 and zinc acetate (GA/F127/zinc acetate = 1/1/0.5, w/w/w) were mixed and mechanically ground by using a high energy hardened steel ball miller with four stainless steel balls added (8000 M Mixer/Mill SPEX Sample Prep). The grinding process was carried out for twenty minutes, resulting in a homogeneous mixture. After milling, the mixture was heated under N_2 atmosphere (100 mL/min) in a tubular fixed-bed oven (OTF-1200X MTI Corporation). The oven was heated to 400 °C with a ramp of 5 °C/min and kept at the targeted temperature for 1 h for the removal of the Pluronic surfactant F127. The oven temperature was then increased to 950 °C at the same heating rate and the temperature was kept constant for another 1 h for the evaporation of metallic Zn. The material was purified with a 3 M HCl solution in an ultrasound bath for 30 min. The porous carbon was obtained after washed with distillated water until pH 7 and was named as MC-GA.

A porous carbon with a larger surface area was also produced through a CO_2 activation approach. The obtained MC-GA above was placed in a tubular fixed-bed oven and the oven was heated to 900 °C at a heating rate of 10 °C/min and the temperature was kept constant for 1 h. The activation process was conducted under CO_2 atmosphere (200 mL/min) and the obtained material was named as MC-GA-A.

2.1.1. Material characterizations

Crystal phase: X-Ray diffraction (XRD) patterns were collected on Rigaku SmartLab diffractometer using a Cu Kα radiation (λ = 1.54 Å) at room temperature to reveal the crystal structures of obtained samples. The step scan mode with step size of 1° in 2θ range of 10° −90° has been adopted for the investigation.

Microstructures and element analysis: The morphological information was collected on a scanning electron microscopy (SEM, JEOL ITL-200) with an accelerating voltage of 15 kV and equipped with energy dispersive spectroscopy (EDS) for chemical analysis. The analysis of microstructures was performed on a scanning transmission electron microscope (STEM, Talos F200X G2) with an accelerating voltage of 200 kV.

Composition of active materials: The thermogravimetric analysis (TGA) was conducted on a Thermogravimetric Analyzer (Q500, TA Instruments) to determine the content of sulfur in the cathode active material within a temperature range of 25-450℃ at a heating rate of 5 ℃/min under nitrogen atmosphere.

Pore size and surface area: A Tristar 3000 (Micromeritics Instrument Corporation) automatic gas sorption analyzer was used to determine the porous structure of synthesized samples. Specific surface area (SSA) and pore-size distribution of various carbonaceous materials were calculated from nitrogen adsorption isotherms using the Brunauer-Emmett-Teller

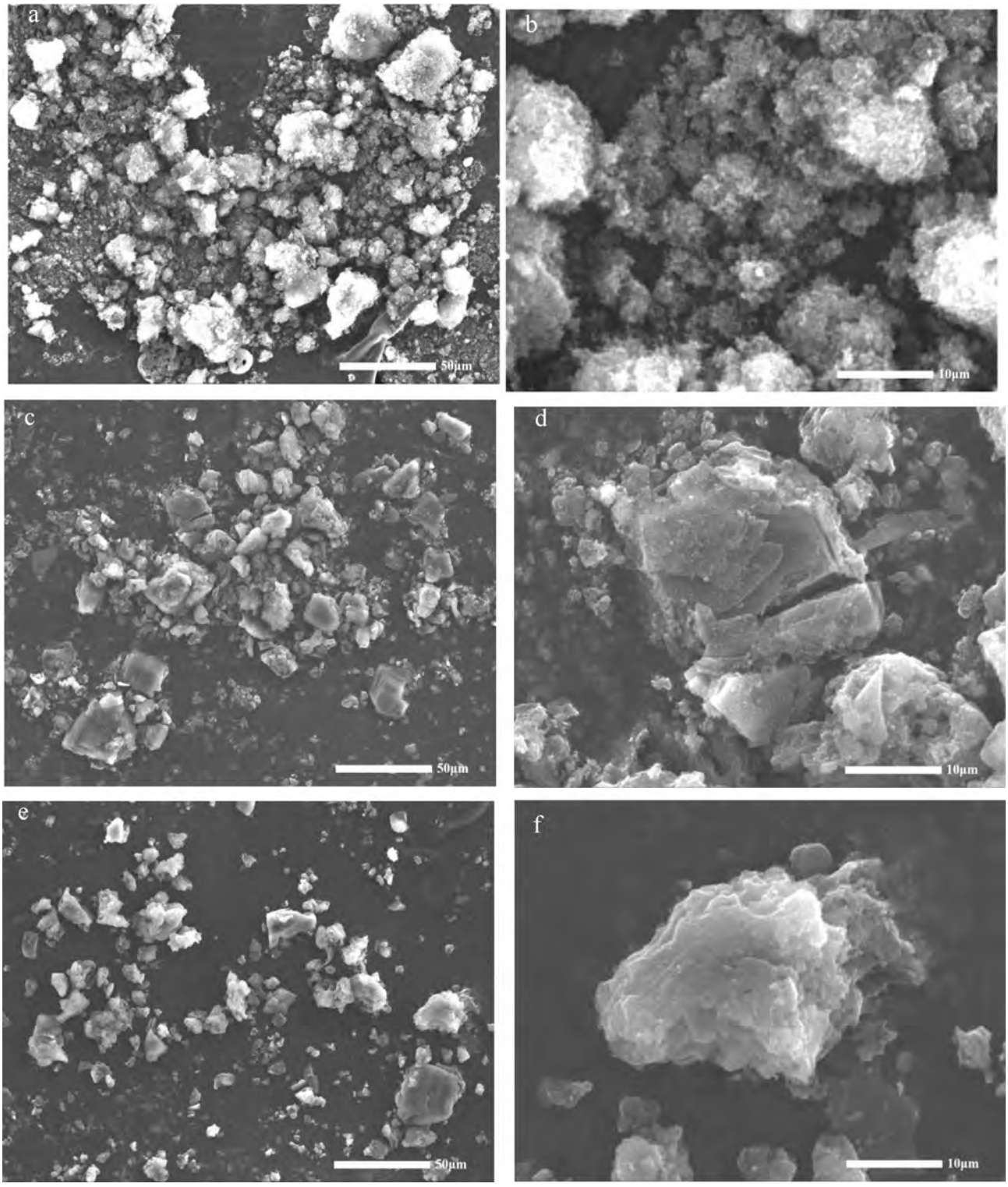

Fig. 3. SEM images of 600JD (a, b), MC-GA (c, d) and MC-GA-A (e, f) with low (a, c, e) and high magnifications (b, d, f).

(BET), and Barrett-Joyner-Halenda (BJH) methods respectively.

Adsorption test: To measure the adsorption capability, 0.2 g tested powders were added into 10 mL electrolyte solution with 1 mM Li_2S_6. The mixtures were stirred for 6 h to have tested sample powders fully contact with Li_2S_6, and then kept at room temperature for 12 h for visual inspections. The Li_2S_6 electrolyte was prepared through mixing Li_2S and elemental sulfur with a stoichiometrically ratio of 1,3-dioxolane (DOL)/ 1,2-dimethoxyethane (DME) (1/1, v/v).

2.1.2. Electrochemical characterizations

Active materials: The synthesized MC-GA and MC-GA-A porous carbons were used as host materials, and the active materials with sulfur impregnated host materials were prepared through a melt-diffusion approach. Typically, 1.1 g commercial sulfur powders and 0.9 g host material were mixed and then ground in an agate mortar. The mixture then was transferred into a glass vessel, sealed, and placed in an oven. The oven was then heated to 155 ℃ and held at the target temperature

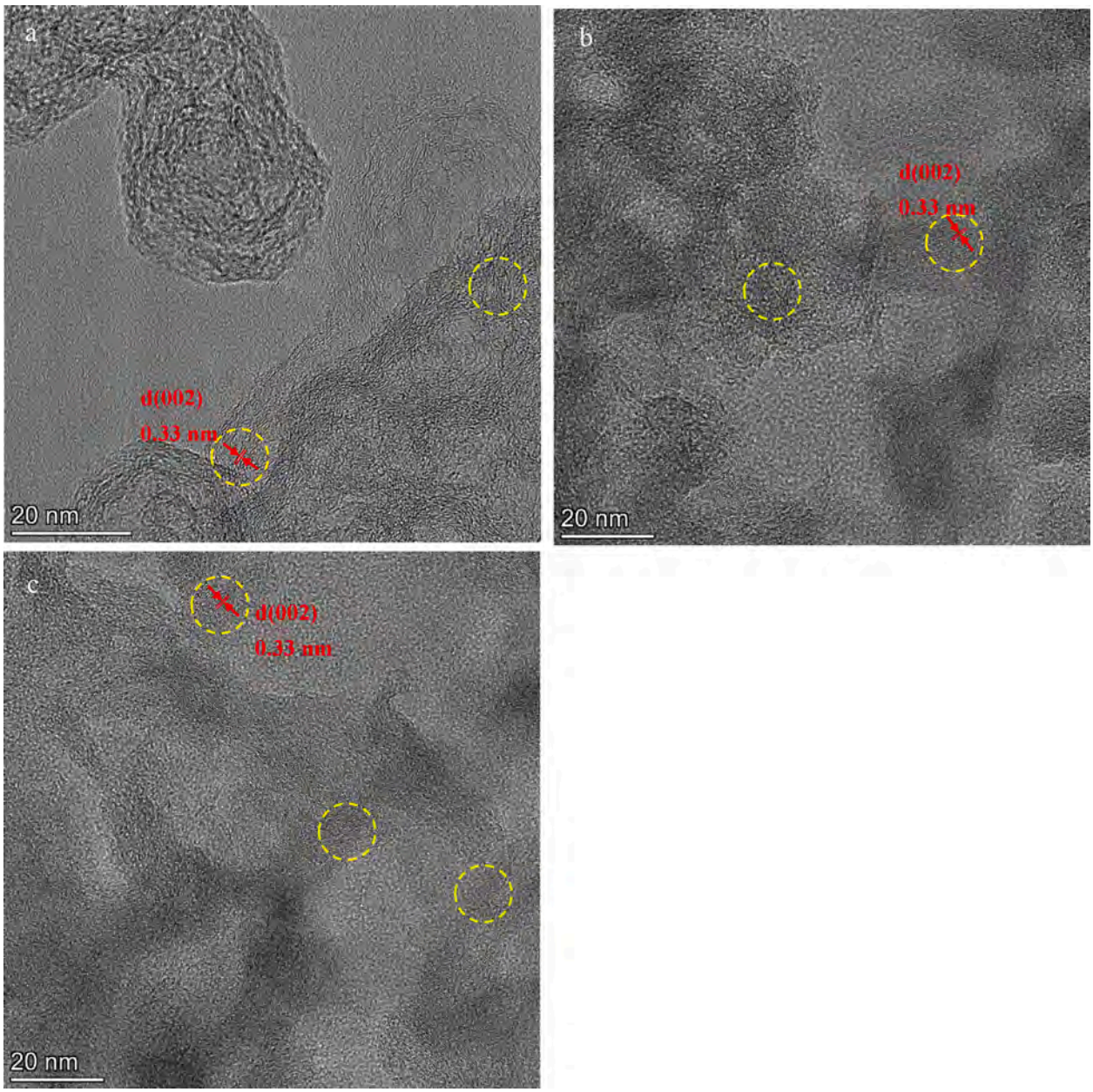

Fig. 4. TEM images of 600JD (a), MC-GA (b) and MC-GA-A (c). Circled regions show the representative domains with clear lattice fringes and the same distance between neighboring fringes, which can be assigned to (0 0 2) plane of crystal graphite phase.

for 12 h. After cooled down to room temperature, the sulfur infiltrated host material was used as the active material for electrode fabrication and further characterizations. For comparison, the same approach was used to prepare the baseline active materials with commercial 600JD carbon as the host material.

Electrode fabrication: The coating slurries were firstly prepared through mixing active material, carbon black (super C45) and binder solution containing polyvinylidene fluoride (PVDF, Solvay) dissolved in 1-Methyl-2-pyrrolidinone (NMP). Typically, the slurry was mixed in a Thinky AR-100 mixer and then was hand-casted onto aluminum foil. The coating on Al foil was then dried at 60 °C for 12 h under vacuum. The dried electrodes were composed of 80% active material, 5% conductive carbon and 15% binder and had the mass loading of around 1.6 mg-S /cm^2.

Cell assembly: The dried electrode was punched into disc with the diameter of 9/16 in. and assembled into coin (CR2032) cells with lithium metal as the counter electrode and polyolefin membrane (Celgard 2325) as separator. The solution containing 1 M lithium bis (trifluoromethane)sulfonimide (LiTFSI) and 2 wt% $LiNO_3$ dissolved in DOL/DME (1/1, v/v) was used as the electrolyte. The cells were assembled inside a glovebox filled with Argon.

Electrochemical characterizations: Galvanostatic cycling tests of assembled cells were conducted on a NEWARE battery tester (BTS-CT-4008) by applying a constant current at room temperature. Initially, three formation cycles with an approximate C/10 current were applied to obtain the exact capacity of the cells for following rate and cycling tests. After the formation cycles, the rate capability of cells was tested following the protocol: charge the cells to 2.8 V with a constant current density of C/10, then discharge to 1.8 V with incremental current densities from 0.1C, 0.2C, 0.5C, 1C to 2C. At each current density, cells underwent three cycles. After the rate test, the cycling test was conducted with the constant current density of 0.5C. The same voltage window of 1.8–2.8 V was applied during the formation, rate and cycling tests.

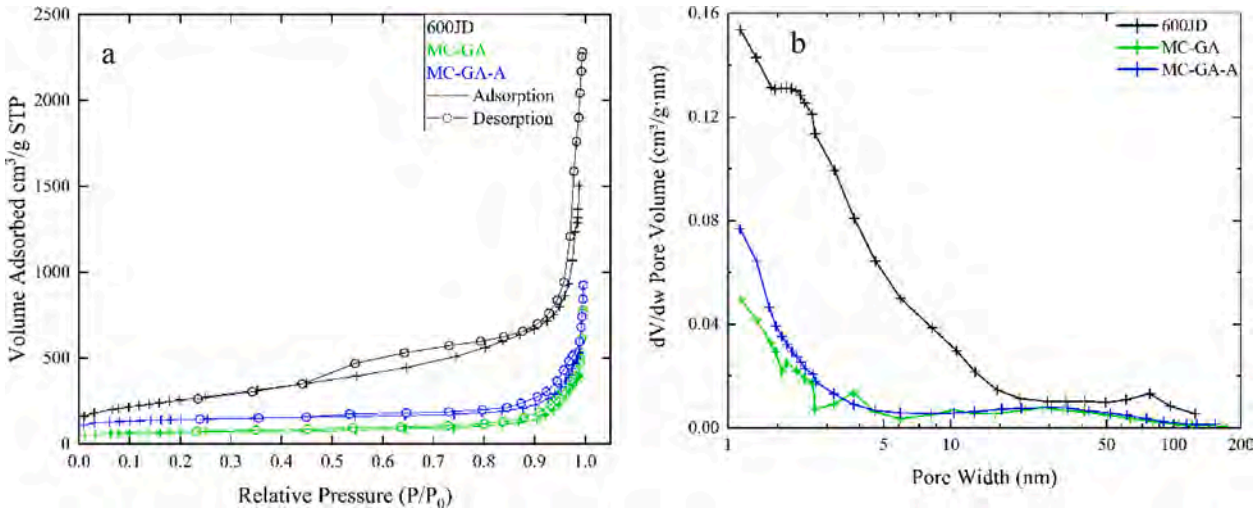

Fig. 5. Nitrogen sorption isotherm plots (a) and pore size distribution (b) of the carbonaceous samples.

Table 1
Structure parameters of the porous carbons.

	Average Pore Diameter (nm)	Pore Volume < 5 nm (P_S, cm^3/g)	Pore Volume >10 nm (P_L, cm^3/g)	Pore Volume Ratio (P_S/P_L)	Total Pore Volume (cm^3/g)	SSA (m^2/g)
600JD	14.5	0.44	1.46	0.30	2.07	868.0
MC-GA	12.0	0.07	0.47	0.15	0.56	257.0
MC-GA-A	8.0	0.08	0.58	0.14	0.69	533.0

Before the formation tests, cyclic voltammetry (CV) tests were conducted on cells using a frequency response analyzer (Gamry, 1010E) with a scanning rate of 0.05 mV/s and voltage range of 1.8–2.8 V.

After the formation tests, electrochemical impedance spectroscopy (EIS) was collected on cells using a frequency response analyzer (Gamry, 1010E) with a potential amplitude of 5 mV over the frequency range from 20 Hz to 1.6 MHz.

3. Results and discussion

After the carbonization process, amorphous carbon products with highly porous architectures can be achieved from the biomass source. XRD patterns (Fig. 2) collected from all samples show two broad diffraction peaks, one located at around 24° and the other at 43°, which correspond to the (002) and (100) crystal planes in graphite respectively assuming a hexagonal crystal system with $P6_3/mmc$ symmetry and the d_{002} spacing of 3.36 Å [37,38]. This implies a predominantly amorphous structure in carbonaceous materials obtained here. Compared with 600JD, the intensity of both broad peaks on XRD patterns obtained from MC-GA and MC-GA-A is relatively higher. This indicates that GA-derived samples have a higher portion of crystalline graphite phase than 600JD does. Besides these two broad peaks, three sharp and weak peaks observed on GA-derived samples can be identified to zinc oxide, which was the residual of zinc acetate introduced into the carbonization process as a crosslinking agent. However, the reflections corresponding to zinc oxide are almost negligible on the XRD pattern obtained from MC-GA-A. This implies that the activation process at high temperature almost removed the zinc component completely, which might release additional small pores in the activated products.

The observations from SEM show that all carbonaceous samples are composed of particles with the size of < 100 nm (Fig. 3**b, 3d and 3f**). These fine particles aggregate together and form 1–50 μm powders with irregular morphology and porous architecture (Fig. 3**a, 3c, and 3e**). The observations from high-resolution TEM (HRTEM) further demonstrate that the aggregation of fine particles generate both < 5 nm (named as small pores thereafter) and > 10 nm (names as large pores thereafter) in the carbonaceous products. Fig. 4 exhibits that numerous small pores and bare large pores can be found in 600JD (Fig. 4**a**). However, MC-GA (Fig. 4**b**) and MC-GA-A (Fig. 4**c**) exhibit both small pores and obvious large pores. In addition, the HRTEM images also confirm the formation of amorphous structure in obtained carbonaceous products. For an individual particle, regions with both clear (circled by yellow dashed lines) and obscure lattice fringes are observable, indicative of the amorphous structure. In further, the distance between neighboring lattice fringes is measured to be 0.33 nm. Given the measuring error, this agrees well with d_{002} spacing of crystalline graphite phase calculated from XRD patterns.

The formation of porous structure is further corroborated through nitrogen sorption measurements. Fig. 5 clearly shows Type-IV isotherms with a hysteresis loop observable for all samples, which is a characteristic of solids with micropores and mesopores. The BJH pore size analysis performed on the adsorption branch of the isotherms shows that two distinct peaks, one below 5 nm (small pores) and the other above 10 nm (large pores), are observable for biomass-derived samples of MC-GA and MC-GA-A. The activation process has little effect on the large pores, but significantly increase the number of small pores. However, it is obvious that 600JD possesses a large number of small pores. Table 1 summarizes the pore structure properties of these carbonaceous samples including average pore sizes, pore volumes and surface area. The activation significantly reduces the average pore size of GA-derived carbon from ~12 nm to ~8 nm and increases the pore volume of large pores. However, the activation has little effect on the pore volume of small pores and volume ratio of small to large pores. The SSA, calculated by the BET method, is 257 m^2/g for MC-GA and it increases to 533 m^2/g for activated MC-GA-A. The higher surface area is the result of more small pores in MC-GA-A generated through the activation process. Otherwise, more large pores in MC-GA-A will result in the lower surface area. The large number of small pores also results in 600JD with a high surface area (868 m^2/g). Among all samples, 600JD has the highest average pore size, pore volume ratio and SSA. However, the volume ratio of small to large pores in both MC-GA and MC-GA-A is ~ 0.15 for both biomass-derived carbons, which is about half of that in 600JD. Given the different roles of large and small pores in the mass transport and polysulfide confinement, it is rational to expect that, used as host materials, the biomass-derived carbons with appropriate distribution of pores will

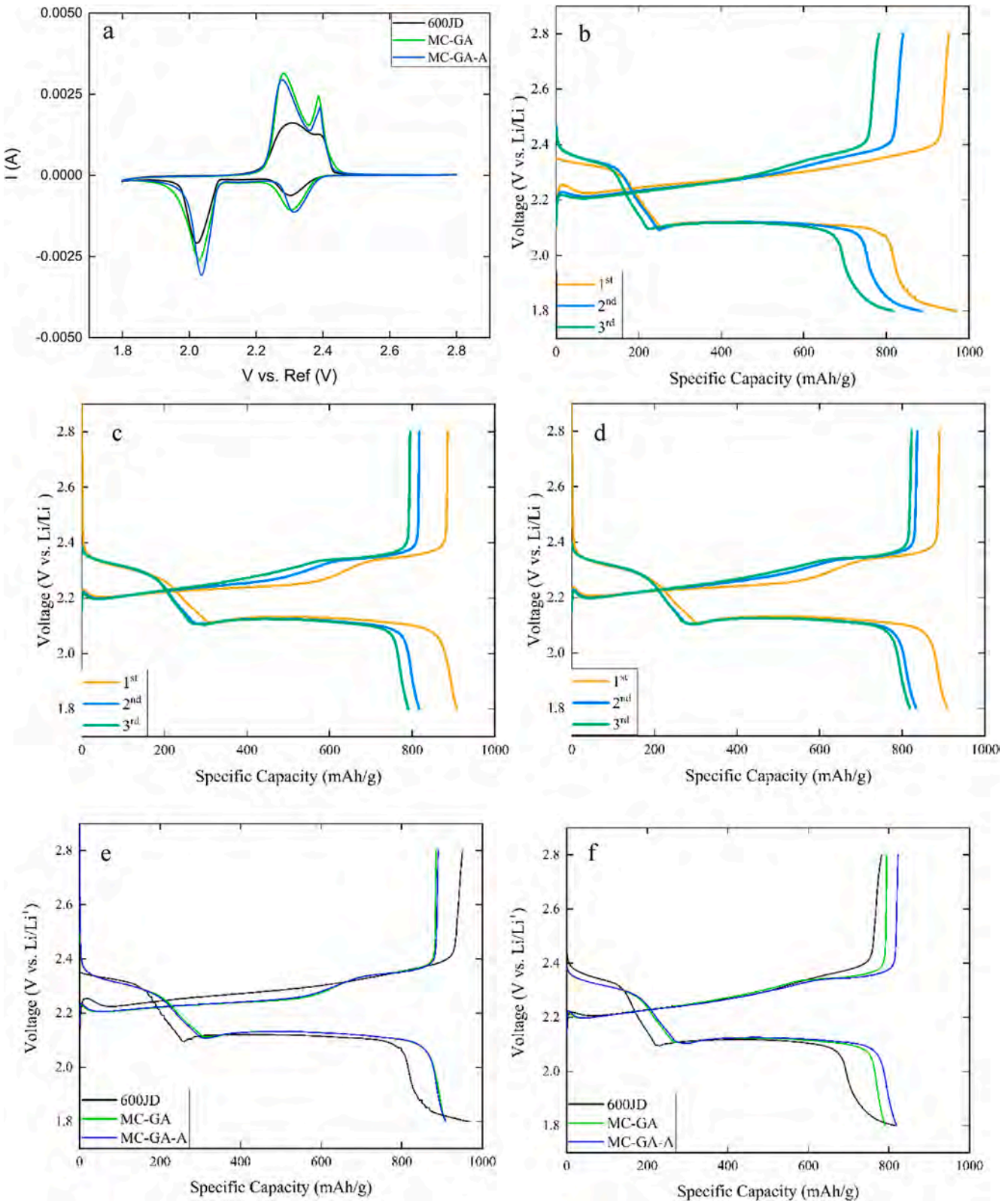

Fig. 6. The CV curves (a) and voltage profiles of LSBs with 600JD (b), MC-GA(c) and MC-GA-A(d) during formation tests. The comparison of LSB performance during first (e) and third (f) formation cycles. The CVs were collected on cells before formations with the scanning rate of 0.05 mV/s.

enable LSBs with excellent electrochemical performance.

The promises of biomass-derived carbons can be observed from their advantages as host materials of sulfur cathodes in improving the LSB performance. Fig. 6**a** shows the CV curves of freshly assembled LSB cells in the initial scans. All hosts present a remarkable reduction peak at ~2.28 V (vs Li^+/Li) followed by second one at ~2.03 V (vs. Li^+/Li), corresponding to the S_8 to polysulfide (S_n^{2-}, $4 \leq n \leq 8$) and then to lower order polysulfides, in the cathodic scans [39]. In the subsequent anodic scans, two peaks, one at ~2.23 V (vs. Li^+/Li) and the other at ~2.38 V (Li^+/Li) are observed, corresponding to the conversion of Li_2S_2 or Li_2S

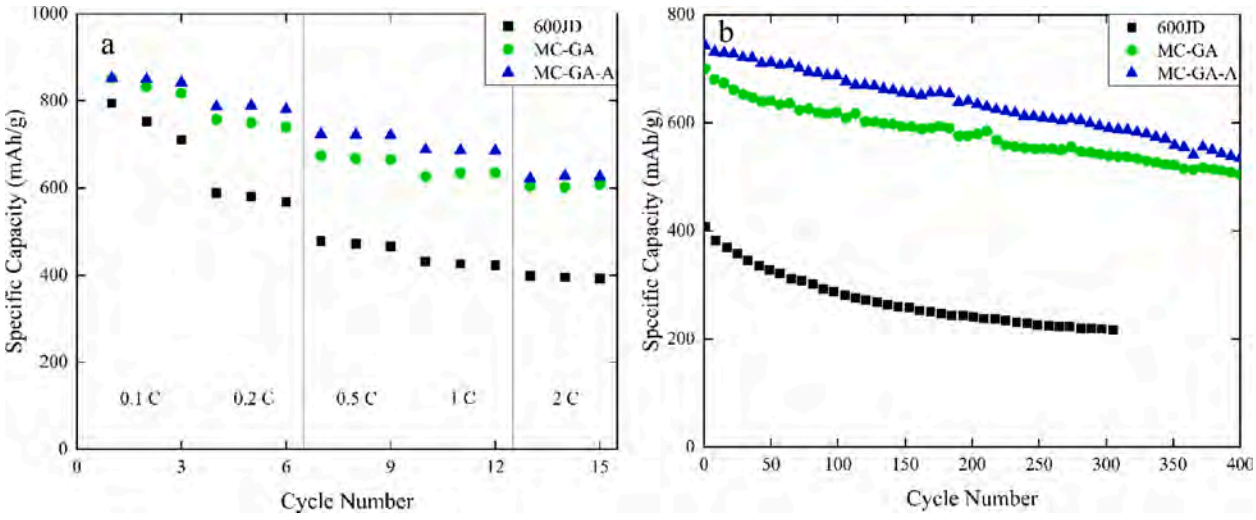

Fig. 7. Rate capability (a) and cycling performance (b) of LSBs with various carbon hosts.

Table 2
Performance comparison of lithium-sulfur batteries with the state-of-the-art biomass-based carbon hosts.

Source	Sulfur loading (mg/cm^2)	Initial discharge capacity (mAh/g)	Cycle number	Capacity of final cycle (mAh/g)	Cycling rate	References
Litchi shell	0.8–0.96	1105 (0.1C)	800	430	1C	[42]
Coconut shell	0.78	1500 (0.1C)	400	517	2C	[43]
Pomegranate residue	2.1	1010 (0.1C)	500	550	0.2C	[44]
Banana peel	1.96	1200 (0.2C)	500	570	1C	[45]
Tea waste	1.2–1.5	744 (0.5C)	100	499	0.5C	[46]
Soybeans	2.0	950 (0.1C)	800	460	0.5C	[47]
Tobacco stems	1.1	1074 (0.1C)	100	745	0.2C	[48]
Yam	1.0–1.1	1556 (0.2C)	450	401.2	1C	[49]
Ferns	N/A	1377 (0.1C)	100	500	0.2C	[50]
Wood chips	1.17–3.33	1302 (0.1C)	50	843	0.1C	[51]
Yeast	1.12	800 (0.1C)	100	642.7	1C	[52]
Garlic acid	1.6	910 (0.1C)	400	590	0.5C	This work

into soluble polysulfides and element sulfur respectively. Compared with 600JD, GA-derived hosts have CV peaks with higher intensity, the right-shifted cathodic peaks, and the left-shifted anodic peaks. The observations from CV measurements agree well with results obtained from the initial formation tests on LSBs. Fig. 6**b to 6d** show that all LSBs demonstrate two plateaus at ~2.4 V (vs. Li^+/Li) and ~2.1 V (Li^+/Li) in the discharge processes, two plateaus at ~2.2 V (vs. Li^+/Li) and ~2.3 V (Li^+/L). During the initial cycle, cells with GA-derived hosts exhibit overlapped voltage profiles, but slightly lower overpotential at the 2.1 V plateau during the discharge process and at the 2.2 V plateau during the charge process than the cell with 600JD (Fig. 6**e**). All these are consistent with observations from the CV measurements. The lower overpotential in the initial cathodic (discharge process of cell) and anodic (charge process of cell) sweeps might be attributed to the reduced polarization caused by the unique porous structure of GA-derived hosts with improved sulfur distribution, better contacts between sulfur and hosts, and higher conductivity of cathodes. The conversion-dissolution-diffusion process of the sulfur and polysulfides in the initial cycle can rearrange the distribution of sulfur and lower the influence of the host on the conductivity of the cathodes [40]. The relatively higher ratio of crystalline graphite phase might also be a beneficial factor to reduce the polarization of cells with GA-derived hosts in the initial, given the high electronic conductivity of graphite [41], but its contribution might not be significant since all cells have almost overlapped voltage curves at every plateau during the third formation cycle (Fig. 6**f**). In the presence of baseline 600JD, the LSB can deliver a relatively higher capacity of ~1000 mAh/g during the initial discharge process (Fig. 6**b and 7d**), while ~910 mAh/g by both biomass-derived carbons (Fig. 6**c to 6e**). This implies the excellent dispersity and high utilization of sulfur in all hosts with high surface area. After three formation cycles, cells with MC-GA-A and 600JD retain the capacity of ~820 mAh/g and ~800 mAh/g in MC-GA (Fig. 6**f**). In other words, >87% of initial capacity is preserved in LSBs with both biomass-derived carbon hosts, while ~82% for baseline 600JD, after three formation cycles. Particularly, >90% of initial capacity is retained in cells with the activated carbon of MC-GA-A. The higher capacity retention might be associated with the strong affinity of unique porous architecture in biomass-derived carbons to sulfur and polysulfides, which will be discussed below.

The superiority of biomass-based carbon hosts can also be found from the promising rate capacity and durability of LSBs. Irrespective of the host materials, the specific capacity delivered by LSBs decreases with the enhancement of current density. The specific capacity delivered by MC-GA-A is 843, 782, 721, 686 and 626 mAh/g at the current density of 0.1C, 0.2C, 0.5C, 1C and 2C respectively (Fig. 7**a**). The capacity delivered by MC-GA cathode is slightly lower. However, the capacity delivered by 600JD cathode drops dramatically from ~800 mAh/g at 0.1C to ~466 mAh/g at 0.5C and decreases gradually to ~400 mAh/g at 2C (Fig. 7**a**). The advantages of biomass-derived carbon hosts can also be observed from the superior durability of LSBs (Fig. 7**b**). After 50 cycles, LSBs with 600JD exhibit only ~326 mAh/g, which is ~80% of the initial capacity and further decreases to <70% after 100 cycles (Fig. 7**b**). However, biomass-derived carbon hosts can retain 80% of the initial capacity (~600 mAh/g) after 200 cycles. Especially, the activated MC-GA-A can deliver the highest capacity of ~720 mAh/g after 200 cycles and retain 80% of the initial capacity (~590 mAh/g) after 400 cycles. Table 2 summarizes the performance of LSBs with hosts obtained in this work and the representative biomass-derived carbon hosts reported by other researchers to date [42–52]. To the best of our knowledge, it is the

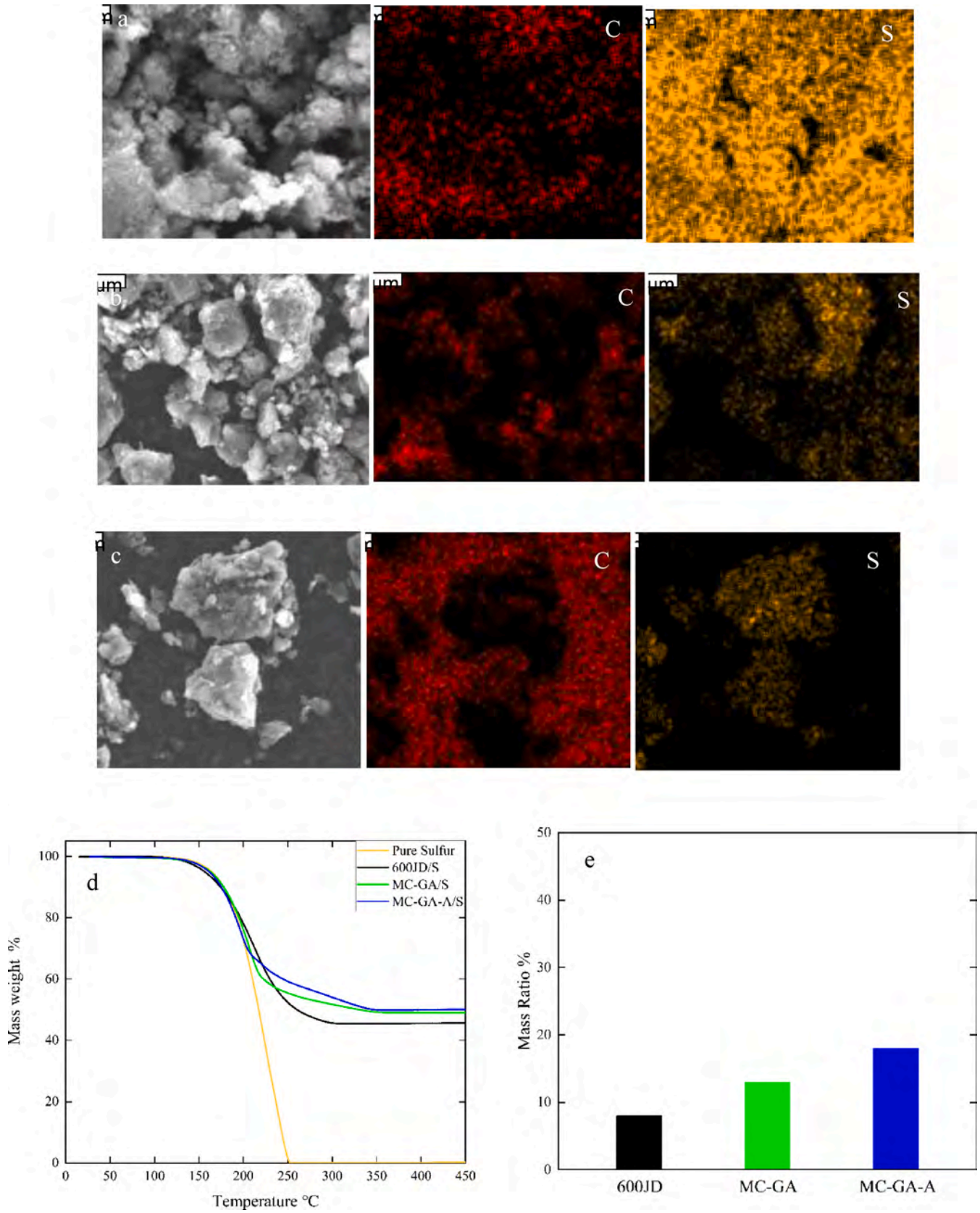

Fig. 8. SEM images and corresponding element mapping images active materials with of 600 JD (a), MC-GA (b) and MC-GA-A (c) hosts. TGA curves (d) of active materials, and the mass weight of sulfur (e) infiltrated in small pores in different carbon hosts.

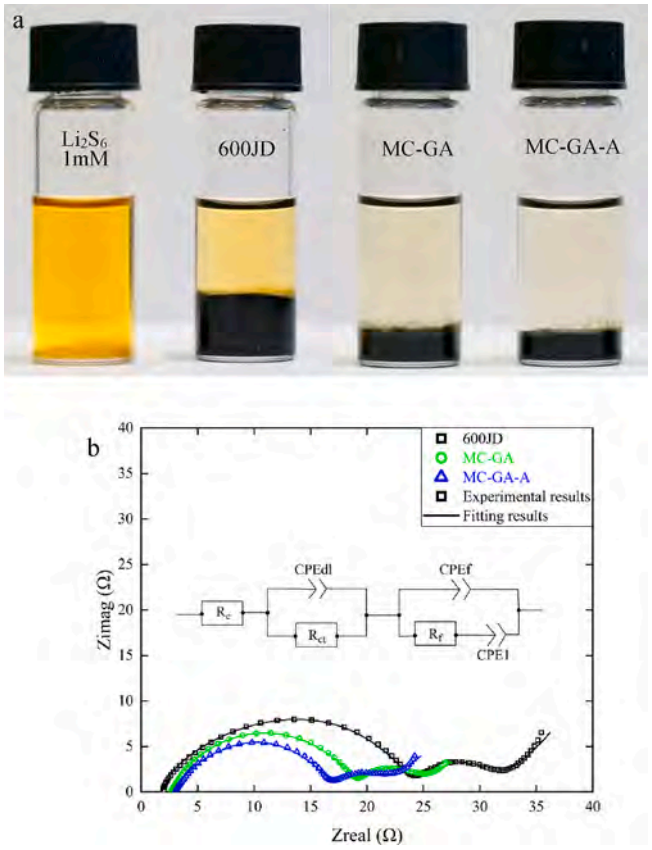

Fig. 9. Photographs (a) of sealed vials of Li_2S_6 solution intact with various carbon hosts for 12 h and Nyquist plots (b) recorded by EIS of cells with different carbon hosts after 3 formation cycles. The inset in b is the equivalent circuit for data fitting.

Table 3
Fitted values for the equivalent circuit elements by simulations of impedance spectra in Fig. 9b.

	R_e (Ω)	R_{ct} (Ω)	R_f (Ω)
600JD	1.81	22.46	7.74
MC-GA	2.71	16.45	5.54
MC-GA-A	3.04	14.05	5.07

first time to report such high capacity retention of a LSB with mere biomass-derived porous carbon hosts [25,53,54], and it is even comparable to those with catalytic hosts [55–59]. It is worthy to note that the zinc oxide in the GA-derived hosts might have little effect on the LSB performance since MC-GA-A demonstrated the best performance with the highest capacity, rate capability and durability here. Otherwise, the MC-GA host with more zinc oxide can demonstrate the best battery performance.

To better understand the effect of biomass-derived carbon hosts on the improved LSB performance, the chemical analysis and TGA measurements were conducted on active materials. The element mapping images (Fig. 8**a to 8c**) demonstrate no elemental sulfur observable between carbon particles, indicating that no sulfur was left outside the particles of all carbon hosts. TGA (Fig. 8**d**) results show that all active materials contained ~50 wt% sulfur. In addition, the sublimation of pure sulfur exhibits a single-slope-like curve, which starts at ~150 °C and ends at ~250 °C. However, a two-slope-like feature, one steep in the region of 150 °C – 250 °C and the other gentle in the region of 250 °C–400 °C, is observable for all active materials with carbon hosts. It is believed that appearance of steep slope corresponding to the volatilization of sulfur from large pores in carbon hosts, while gentle one from small pores [60,61]. The steeper the slope, the easier the volatilization of sulfur from the host. When the temperature is below 250 °C, TGA curves obtained from all active materials almost overlap with that of pure sulfur, indicating the negligible affinity of large pores in the hosts to sulfur. The amount of sulfur contained in small and large pores can be calculated based on the mass weight losses occurred in two temperature regions. Fig. 8**e** shows that MC-GA-A has ~18 wt% sulfur (50 wt% in total) filled in small pores, ~13 wt% for MC-GA, and only ~8 wt% for 600JD. This suggests that the small pores have strong confinement on sulfur. However, too low ratio of large to small pores might retard the diffusion of sulfur and lower the utilization of small pores in 600JD particles for sulfur accommodation. However, the appropriate distribution of pores in biomass-derived carbons benefits the sulfur infiltration into small pores. The high accessibility of small pores to sulfur benefits can benefit the ion transport in the sulfur cathode and thus the high utilization of sulfur at high rates. This is corroborated by the superior rate capability of LSBs with GA-derived carbon hosts over those with the baseline 600JD.

The biomass-derived carbons do not only trap sulfur, but also have the capability to anchor polysulfides. The observations from adsorption measurements (Fig. 9**a**) demonstrate that, after contact with biomass-derived carbons, the yellowish coloration of Li_2S_6 solution diminished. From 600JD to MC-GA and MC-GA-A, the yellowish coloration becomes lighter, indicating the strongest affinity of MC-GA-A to the polysulfides. It has been well recognized that the porous structure of the host plays a crucial role in determining the affinity of host materials, in which the small pores provide sites to anchor polysulfides while large pores for fast mass transport [25]. Although having the highest pore volume of small pores (Fig. 5 and Table 1), too few large pores retard the polysulfide diffusion and lower the utilization of small pores in 600JD particles to trap the polysulfides. Observations from TGA and adsorption measurements agree well with results from nitrogen sorption that MC-GA-A has a suitable ratio of large to small pores and appropriate number of small pores. The strong affinity of cathodes can also benefit the kinetics of polysulfide conversion. This was corroborated by the EIS measurements (Fig. 9**b**). Regardless of hosts employed, EIS spectra collected from all LSBs are composed of two depressed semicircles and an inclined line. The semicircle in the high-frequency region is generally related to the charge-transfer process (R_{ct}/CPE_{dl}) at the interface between conductive agent and the electrolyte, while the other in the middle-frequency region associated with the formation of solid-electrolyte-interface (SEI) films (R_f/CPE_f) [62]. The inclined line in low-frequency region ascribed to the diffusion of ions (CPE_{diff}) in the sulfur cathode. With the assistance of the equivalent circuit (insert in Fig. 9**b**), the simulated results show that the ohmic resistance (R_e) in both biomass-derived carbons is almost identical and slightly higher than that of 600JD (Table 3). This indicates the excellent electronic conductivity in all sulfur cathodes. However, MC-GA-A sulfur cathode has the lowest value of R_{ct} (14.05 Ω), while 16.45 Ω is for MC-GA and 22.46 Ω is for 600JD. Similar result can be found on R_f for all LSBs. Lower R_{ct} indicates better accessibility of active material in biomass-derived carbon sulfur cathodes. Lower R_f implies that cathodes with biomass-derived carbons have thinner SEI films with less soluble polysulfides than that with 600JD. Thus, results from TGA, absorption measurement and EIS spectra confirm that the appropriate porous structure in biomass-derived carbons promotes both affinity of cathodes to sulfur/polysulfides and mass transport, leading to the significantly improved LSB performance.

4. Conclusions

Low cost and highly porous carbons were successfully prepared from biomass sources. Using as hosts of cathodes in LSBs, the biomass-based carbons deliver a high reversible capacity of > 800 mAh/g and retain > 80% of initial capacity after 200 cycles. Especially, the activated carbons exhibited 80% capacity retention after 400 cycles. The promising LSB

performance can be ascribed to the unique porous architecture of biomass-based carbons. The small pores in biomass-based carbons can provide more sites to anchor sulfur and polysulfides, while large pores provide channels for fast transport of ions.

CRediT authorship contribution statement

Jian Yang: Investigation, Data curation, Writing – original draft. **Guanyi Wang:** Investigation. **Ana Paula Teixeira:** Writing – review & editing. **Glaura Goulart Silva:** Writing – review & editing. **Zachary Hansen:** Investigation. **Maruj Jamal M Jamal:** Investigation. **Kevin Mathew:** Validation, Data curation. **Jie Xiong:** Validation, Data curation. **Tiffany Zhou:** Validation. **Michal Mackowiak:** Resources, Project administration. **Paul Dan Fleming:** Writing – review & editing. **Qingliu Wu:** Conceptualization, Methodology, Supervision, Writing – review & editing.

Declaration of Competing Interest

The authors declare that they have no known competing financial interests or personal relationships that could have appeared to influence the work reported in this paper.

Data availability

Data will be made available on request.

Acknowledgement

This work was supported by the Xponential Battery Materials B. V. (“XBM”). The authors are also grateful for the carbon materials from Centro de Tecnologia em Nanomateriais e Grafeno CTNano at Federal University of Minas Gerais. This work made use of the Talos F200X G2 S/TEM that is funded in part through NSF MRI award #2018587.

References

[1] L. Borchardt, M. Oschatz, S. Kaskel, Carbon materials for lithium sulfur batteries-ten critical questions, Chem. Eur. J. 22 (2016) 7324–7351.
[2] Z.-L. Xu, J.-K. Kim, K. Kang, Carbon nanomaterials for advanced lithium sulfur batteries, Nano Today 19 (2018) 84–107.
[3] A. Fu, C. Wang, F. Pei, J. Cui, X. Fang, N. Zheng, Recent advances in hollow porous carbon materials for lithium–sulfur batteries, Small 15 (2019) 1804786–1804806.
[4] L. Zhang, Y. Wang, Z. Niu, J. Chen, Advanced nanostructured carbon-based materials for rechargeable lithium-sulfur batteries, Carbon 141 (2019) 400–416.
[5] M. Zheng, Y. Chi, Q. Hu, H. Tang, X. Jiang, L. Zhang, S. Zhang, H. Pang, Q. Xu, Carbon nanotube-based materials for lithium–sulfur batteries, J. Mater. Chem. A 7 (2019) 17204–17241.
[6] R. Fang, K. Chen, L. Yin, Z. Sun, F. Li, H.M. Cheng, The regulating role of carbon nanotubes and graphene in lithium-ion and lithium–sulfur batteries, Adv. Mater. 31 (2019) 1800863–1800884.
[7] J. Ren, Y. Zhou, L. Xia, Q. Zheng, J. Liao, E. Long, F. Xie, C. Xu, D. Lin, Rational design of a multidimensional N-doped porous carbon/MoS 2/CNT nano-architecture hybrid for high performance lithium–sulfur batteries, J. Mater. Chem. A 6 (2018) 13835–13847.
[8] Q. Zhang, N. Huang, Z. Huang, L. Cai, J. Wu, X. Yao, CNTs@ S composite as cathode for all-solid-state lithium-sulfur batteries with ultralong cycle life, J. Energy Chem. 40 (2020) 151–155.
[9] Y. Wang, R. Zhang, J. Chen, H. Wu, S. Lu, K. Wang, H. Li, C.J. Harris, K. Xi, R. V. Kumar, Enhancing catalytic activity of titanium oxide in lithium–sulfur batteries by band engineering, Adv. Energy Mater. 9 (2019) 1900953–1900963.
[10] J. Hou, X. Tu, X. Wu, M. Shen, X. Wang, C. Wang, C. Cao, H. Pang, G. Wang, Remarkable cycling durability of lithium-sulfur batteries with interconnected mesoporous hollow carbon nanospheres as high sulfur content host, Chem. Eng. J. 401 (2020) 126141–126151.
[11] J. Zhang, Z. Chen, G. Wang, L. Hou, C. Yuan, Eco-friendly and scalable synthesis of micro-/mesoporous carbon sub-microspheres as competitive electrodes for supercapacitors and sodium-ion batteries, Appl. Surf. Sci. 533 (2020) 147511–147520.
[12] G.D. Park, D.S. Jung, J.-K. Lee, Y.C. Kang, Pitch-derived yolk-shell-structured carbon microspheres as efficient sulfur host materials and their application as cathode material for Li–S batteries, Chem. Eng. J. 373 (2019) 382–392.
[13] S. Choudhury, P. Srimuk, K. Raju, A. Tolosa, S. Fleischmann, M. Zeiger, K. I. Ozoemena, L. Borchardt, V. Presser, Carbon onion/sulfur hybrid cathodes via inverse vulcanization for lithium–sulfur batteries, Sustain, Energy Fuels 2 (2018) 133–146.
[14] S.-H. Chung, A. Manthiram, Low-cost, porous carbon current collector with high sulfur loading for lithium–sulfur batteries, Electrochem. Commun. 38 (2014) 91–95.
[15] Y. Cui, Q. Zhang, J. Wu, X. Liang, A.P. Baker, D. Qu, H. Zhang, H. Zhang, X. Zhang, Developing porous carbon with dihydrogen phosphate groups as sulfur host for high performance lithium sulfur batteries, J. Power Sources 378 (2018) 40–47.
[16] H. Shi, W. Lv, C. Zhang, D.W. Wang, G. Ling, Y. He, F. Kang, Q.H. Yang, Functional carbons remedy the shuttling of polysulfides in lithium–sulfur batteries: confining, trapping, blocking, and breaking up, Adv. Funct. Mater. 28 (2018) 1800508–1800528.
[17] C. Schneidermann, C. Kensy, P. Otto, S. Oswald, L. Giebeler, D. Leistenschneider, S. Grätz, S. Dörfler, S. Kaskel, L. Borchardt, Nitrogen-doped biomass-derived carbon formed by Mechanochemical synthesis for lithium–sulfur batteries, ChemSusChem 12 (2019) 310–319.
[18] Y. Liu, Y. Fang, Z. Zhao, C. Yuan, X.W. Lou, A ternary Fe1− xS@ porous carbon nanowires/reduced graphene oxide hybrid film electrode with superior volumetric and gravimetric capacities for flexible sodium ion batteries, Adv. Energy Mater. 9 (2019) 1803052–1803060.
[19] J. Xu, T. Lawson, H. Fan, D. Su, G. Wang, Updated metal compounds (MOFs, - S, -OH, -N, -C) used as cathode materials for lithium-sulfur batteries, Adv. Energy Mater. 8 (2018) 1702607–1702629.
[20] P. Geng, S. Zheng, H. Tang, R. Zhu, L. Zhang, S. Cao, H. Xue, H. Pang, Transition metal sulfides based on graphene for electrochemical energy storage, Adv. Energy Mater. 8 (2018) 1703259–1703284.
[21] F. Ma, J. Liang, T. Wang, X. Chen, Y. Fan, B. Hultman, H. Xie, J. Han, G. Wu, Q. Li, Efficient entrapment and catalytic conversion of lithium polysulfides on hollow metal oxide submicro-spheres as lithium–sulfur battery cathodes, Nanoscale 10 (2018) 5634–5641.
[22] F. Qi, Z. Sun, X. Fan, Z. Wang, Y. Shi, G. Hu, F. Li, Tunable Interaction between Metal-Organic Frameworks and Electroactive Components in Lithium-Sulfur Batteries: Status and Perspectives, Adv. Energy Mater. 11 (2021) 2100387–2100411.
[23] X.-J. Hong, C.-L. Song, Y. Yang, H.-C. Tan, G.-H. Li, Y.-P. Cai, H. Wang, Cerium based metal–organic frameworks as an efficient separator coating catalyzing the conversion of polysulfides for high performance lithium–sulfur batteries, ACS Nano 13 (2019) 1923–1931.
[24] Q. Li, Y.P. Liu, Y. Wang, Y.X. Chen, X.D. Guo, Z.G. Wu, B.H. Zhong, Review of the application of biomass-derived porous carbon in lithium-sulfur batteries, Ionics 26 (2020) 4765–4781.
[25] A. Benitez, J. Amaro-Gahete, Y.C. Chien, A. Caballero, J. Morales, D. Brandell, Recent advances in lithium-sulfur batteries using biomass-derived carbons as sulfur host, Renew. Sust. Energ. Rev. 154 (2022) 111783–111812.
[26] S.C. Wei, H. Zhang, Y.Q. Huang, W.K. Wang, Y.Z. Xia, Z.B. Yu, Pig bone derived hierarchical porous carbon and its enhanced cycling performance of lithium-sulfur batteries, Energy Environ. Sci. 4 (2011) 736–740.
[27] S.T. Zhang, M.B. Zheng, Z.X. Lin, N.W. Li, Y.J. Liu, B. Zhao, H. Pang, J.M. Cao, P. He, Y. Shi, Activated carbon with ultrahigh specific surface area synthesized from natural plant material for lithium-sulfur batteries, J. Mater. Chem. A 2 (2014) 15889–15896.
[28] S. Xin, L. Gu, N.H. Zhao, Y.X. Yin, L.J. Zhou, Y.G. Guo, L.J. Wan, Smaller sulfur molecules promise better lithium-sulfur batteries, J. Am. Chem. Soc. 134 (2012) 18510–18513.
[29] J. Zhou, Y. Guo, C. Liang, J. Yang, J. Wang, Y. Nuli, Confining small sulfur molecules in peanut shell-derived microporous graphitic carbon for advanced lithium sulfur battery, Electrochim. Acta 273 (2018) 127–135.
[30] S.H. Chung, A. Manthiram, Carbonized eggshell membrane as a natural polysulfide reservoir for highly reversible Li-S batteries, Adv. Mater. 26 (2014) 1360–1365.
[31] S.H. Chung, C.H. Chang, A. Manthiram, A carbon-cotton cathode with ultrahigh-loading capability for statically and dynamically stable lithium-sulfur batteries, Acs Nano 10 (2016) 10462–10470.
[32] M.K. Rybarczyk, H.J. Peng, C. Tang, M. Lieder, Q. Zhang, M.M. Titirici, Porous carbon derived from rice husks as sustainable bioresources: insights into the role of micro-/mesoporous hierarchy in hosting active species for lithium-sulphur batteries, Green Chem. 18 (2016) 5169–5179.
[33] C. Hernandez-Rentero, R. Cordoba, N. Moreno, A. Caballero, J. Morales, M. Olivares-Marin, V. Gomez-Serrano, Low-cost disordered carbons for Li/S batteries: A high-performance carbon with dual porosity derived from cherry pits, Nano Res. 11 (2018) 89–100.
[34] B. Boye, E. Brillas, A. Buso, G. Farnia, C. Flox, M. Giomo, G. Sandona, Electrochemical removal of gallic acid from aqueous solutions, Electrochim. Acta 52 (2006) 256–262.
[35] R. Correcher, Y. Budyk, A. Fullana, Role of gallic acid in the synthesis of carbon-encapsulated iron nanoparticles by hydrothermal carbonization: selecting iron oxide composition, ACS Omega 6 (2021) 29547–29554.
[36] A. Sanchez-Sanchez, M.T. Izquierdo, J. Ghanbaja, G. Medjandi, S. Mathieu, A. Celzard, V. Fierro, Excellent electrochemical performances of nanocast ordered mesoporous carbons based on tannin-related polyphenols as supercapacitor electrodes, J. Power Sources 344 (2017) 15–24.
[37] L. Wang, C. Schütz, G. Salazar-Alvarez, M.-M. Titirici, Carbon aerogels from bacterial nanocellulose as anodes for lithium ion batteries, RSC Adv. 4 (2014) 17549–17554.
[38] A.S. Alex, B. John, Microporous carbon aerogel prepared through ambient pressure drying route as anode material for lithium ion cells, Polym. Adv. Technol. 28 (2017) 1945–1950.

[39] Z.W. Seh, Y. Sun, Q. Zhang, Y. Cui, Designing high-energy lithium–sulfur batteries, Chem. Soc. Rev. 45 (2016) 5605–5634.
[40] M. Sadd, S. De Angelis, S. Colding-Jørgensen, D. Blanchard, R.E. Johnsen, S. Sanna, E. Borisova, A. Matic, J.R. Bowen, Visualization of dissolution-precipitation processes in lithium-sulfur batteries, Adv. Energy Mater. 12 (2022) 2103126–2103137.
[41] I.L. Spain, Electronic transport properties of graphite, carbons, and related materials, in: Chemistry and Physics of Carbon, CRC Press, 2021, pp. 119–304.
[42] S. Zhang, M. Zheng, Z. Lin, N. Li, Y. Liu, B. Zhao, H. Pang, J. Cao, P. He, Y. Shi, Activated carbon with ultrahigh specific surface area synthesized from natural plant material for lithium–sulfur batteries, J. Mater. Chem. A 2 (2014) 15889–15896.
[43] Z.H. Chen, X.L. Du, J.B. He, F. Li, Y. Wang, Y.L. Li, B. Li, S. Xin, Porous coconut shell carbon offering high retention and deep lithiation of sulfur for lithium-sulfur batteries, ACS Appl. Mater. Interfaces 9 (2017) 33855–33862.
[44] X. Chen, G. Du, M. Zhang, A. Kalam, Q. Su, S. Ding, B. Xu, Nitrogen-doped hierarchical porous carbon derived from low-cost biomass pomegranate residues for high performance lithium-sulfur batteries, J. Electroanal. Chem. 848 (2019) 113316–113322.
[45] K. Yang, Q. Gao, Y. Tan, W. Tian, W. Qian, L. Zhu, C. Yang, Biomass-derived porous carbon with micropores and small mesopores for high-performance lithium-sulfur batteries, Chem. Eur. J. 22 (2016) 3239–3244.
[46] T. Zhao, J. Chen, K. Dai, J. Zhang, M. Yuan, X. Li, K. Zhang, J. Zhang, Y. Li, Z. Liu, H. He, B. Li, G. Zhang, Boosted polysulfides regulation by iron carbide nanoparticles-embedded porous biomass-derived carbon toward superior lithium-sulfur batteries, J. Colloid Interface Sci. 605 (2022) 129–137.
[47] G. Ren, S. Li, Z.-X. Fan, J. Warzywoda, Z. Fan, Soybean-derived hierarchical porous carbon with large sulfur loading and sulfur content for high-performance lithium–sulfur batteries, J. Mater. Chem. A 4 (2016) 16507–16515.
[48] M.-E. Zhong, J. Guan, J. Sun, H. Guo, Z. Xiao, N. Zhou, Q. Gui, D. Gong, Carbon nanodot-decorated alveolate N, O, S tridoped hierarchical porous carbon as efficient electrocatalysis of polysulfide conversion for lithium-sulfur batteries, Electrochim. Acta 299 (2019) 600–609.
[49] J.M. Chabu, Y. Li, Y.N. Liu, Biomass-derived N, O, and S-tridoped hierarchically porous carbon as a cathode for lithium−sulfur batteries, ChemNanoMat 5 (2019) 612–618.
[50] X.-L. You, L.-J. Liu, M.-Y. Zhang, M.D. Walle, Y. Li, Y.-N. Liu, Novel biomass derived hierarchical porous carbon for lithium sulfur batteries, Mater. Lett. 217 (2018) 167–170.
[51] C. Schneidermann, C. Kensy, P. Otto, S. Oswald, L. Giebeler, D. Leistenschneider, S. Gratz, S. Dorfler, S. Kaskel, L. Borchardt, Nitrogen-doped biomass-derived carbon formed by mechanochemical synthesis for lithium-sulfur batteries, ChemSusChem 12 (2019) 310–319.
[52] G. Feng, X. Liu, Z. Wu, Y. Chen, Z. Yang, C. Wu, X. Guo, B. Zhong, W. Xiang, J. Li, Enhancing performance of Li–S batteries by coating separator with MnO @ yeast-derived carbon spheres, J. Alloys Compd. 817 (2020) 152723–152732.
[53] S.H. Chung, A. Manthiram, Current status and future prospects of metal–sulfur batteries, Adv. Mater. 31 (2019) 1901125–1901174.
[54] A. Benítez, J. Amaro-Gahete, Y.-C. Chien, Á. Caballero, J. Morales, D. Brandell, Recent advances in lithium-sulfur batteries using biomass-derived carbons as sulfur host, Renew. Sust. Energ. Rev. 154 (2022) 111783–111812.
[55] Q. Sun, B. Xi, J.Y. Li, H. Mao, X. Ma, J. Liang, J. Feng, S. Xiong, Nitrogen-doped graphene-supported mixed transition-metal oxide porous particles to confine polysulfides for lithium-sulfur batteries, Adv. Energy Mater. 8 (2018) 1800595–1800604.
[56] S.F. Ng, M.Y.L. Lau, W.J. Ong, Lithium-sulfur battery cathode design: tailoring metal-based nanostructures for robust polysulfide adsorption and catalytic conversion, Adv. Mater. 33 (2021) 2008654–2008707.
[57] J. Wang, B. Ding, X. Lu, H. Nara, Y. Sugahara, Y. Yamauchi, Single atom-based nanoarchitectured electrodes for high-performance lithium-sulfur batteries, Adv. Mater. Interfaces 8 (2021) 2002159–2002175.
[58] S. Huang, Z. Wang, Y. Von Lim, Y. Wang, Y. Li, D. Zhang, H.Y. Yang, Recent advances in heterostructure engineering for lithium–sulfur batteries, Adv. Energy Mater. 11 (2021) 2003689–2003715.
[59] Y.C. Jiang, H.M.U. Arshad, H.J. Li, S. Liu, G.R. Li, X.P. Gao, Crystalline multi-metallic compounds as host materials in cathode for lithium-sulfur batteries, Small 17 (2021) 2005332–2005350.
[60] L. Li, L. Huang, R.J. Linhardt, N. Koratkar, T. Simmons, Repurposing paper by-product lignosulfonate as a sulfur donor/acceptor for high performance lithium–sulfur batteries, Sustain. Energy Fuels 2 (2018) 422–429.
[61] M. Xiang, Y. Wang, J. Wu, Y. Guo, H. Wu, Y. Zhang, H. Liu, Natural silk cocoon derived nitrogen-doped porous carbon nanosheets for high performance lithium-sulfur batteries, Electrochim. Acta 227 (2017) 7–16.
[62] Z. Zhang, D.H. Wu, Z. Zhou, G.R. Li, S. Liu, X.P. Gao, Sulfur/nickel ferrite composite as cathode with high-volumetric-capacity for lithium-sulfur battery, Sci. China Mater. 62 (2019) 74–86.